Electronic Supplementary Information (ESI) for

Photoluminescent DNA Binding and Cytotoxic Activity of a Platinum(II) Complex Bearing a Tetradentate β-Diketiminate Ligand

Jennifer M. Hope, Justin J. Wilson, and Stephen J. Lippard*

Department of Chemistry, Massachusetts Institute of Technology
Cambridge, MA 02139, USA

Email: lippard@mit.edu

Contents:

Experimental Section

References.

Experimental

General Materials and Methods. All synthetic procedures were carried out with HPLC-grade solvents under normal atmospheric conditions with no measures taken to exclude moisture or oxygen. The ligand, $BDI^{QQ}H\cdot 3HCl\cdot 2H_2O$, was prepared as previously described.[1] The platinum complexes, *cis*-$[Pt(DMSO)_2Cl_2]$[2] and *cis*/*trans*-$[Pt(SMe_2)_2Cl_2]$,[3] were also synthesized by established methods. Other reagents were used as received from commercial vendors. UV-Vis absorbance spectra were collected with a Varian Cary 1E spectrophotometer using a quartz cuvette with a path length of 10 mm and a circulating water bath to control the sample temperature. Fourier transform infrared spectra were acquired with a ThermoNicolet Avatar 360 spectrophotometer running OMNIC software; samples were prepared as KBr plates. Fluorescence data were obtained with a Quanta Master 4L-format scanning spectrofluorimeter from Photon Technology International. Measurements were taken using a quartz cuvette with a path length of 10 mm and a circulating water bath to control the sample temperature. Photoluminescence quantum yields were determined using the equation $\Phi = \Phi_{ref} \times (\nabla/\nabla_{ref}) \times (\eta^2/\eta_{ref}^2)$, where Φ and Φ_{ref} are the quantum yields of the sample and a reference, ∇ and ∇_{ref} are the slopes of linear plots of the absorbance at the excitation wavelength versus the integrated emission intensity, and η and η_{ref} are the refractive indices of the solvents used. Absorbance values at the excitation wavelength were maintained below 0.1 AU for these measurements, and both the sample and reference were excited at 525 nm. The reference used was $[Ru(bpy)_3]Cl_2$ in air-equilibrated water ($\Phi = 0.040$).[4] Emission lifetime measurements were measured after excitation at 550 nm with a sub-picosecond Coherent Libra HE Ti: Sapphire Amplifier System, as previously described.[5] A Hamamatsu C4334 Streak Scope streak camera fitted with a 570 nm long pass filter to exclude scattered excitation light was used to measure the transient emission decay with the spectral window centered at 650 nm. NMR spectra were obtained using a Bruker AVANCE-400 MHz spectrometer with a variable temperature probe in the Department of Chemistry Instrumentation Facility (DCIF) of MIT. ^{1}H NMR resonances were referenced internally to solvent versus $SiMe_4$ ($\delta = 0.00$ ppm), and chemical shifts are reported in ppm. 2-D DOSY NMR spectra were acquired using the ledgp2s Bruker pulse sequence with a diffusion delay, Δ, of 0.1 s and a gradient length, δ, of 2.5 ms. Dynamic light scattering measurements were obtained with a DynaPro NanoStar light scatterer. Samples were centrifuged at 5000 rpm for 5 min prior to analysis to remove scattering interference from particulates, and sample temperatures were maintained at 25 °C with a circulating water bath. Mass spectrometric data were collected using an Agilent Technologies 1100 series LC-MSD trap. Electrochemical data were acquired with a VersaSTAT3 potentiostat from Princeton Applied Research and the V3 Studio software. A three-electrode system was used, consisting of a silver/silver chloride reference, a glassy carbon working electrode, and a platinum wire auxiliary electrode. Samples were prepared as 2 mM solutions in DMF with 0.1 M (n-$Bu_4N)PF_6$ as the supporting electrolyte. Cyclic voltammograms were obtained at a scan rate of 20 mV/s or 100 mV/s, and the external ferrocene/ferrocenium redox couple was consistently observed between 0.54 and 0.56 V vs. Ag/AgCl. Concentrations of the Pt-containing solutions for DNA titrations, extinction coefficient measurements, and cytotoxicity assays were determined by graphite furnace atomic absorption spectroscopy (GFAAS). A Perkin-Elmer AAnalyst 600 GFAAS was used.

Synthesis of $[Pt(BDI^{QQ})]Cl\cdot 2H_2O$ from *cis*-$[Pt(DMSO)_2Cl_2]$. To a suspension of 167 mg (0.356 mmol) of $BDI^{QQ}H\cdot 3HCl\cdot 3H_2O$ in ca. 2 mL acetonitrile (MeCN) were added approximately 1 mL of triethylamine (TEA) in a dropwise manner, forming a homogeneous solution. To this orange solution was added 150 mg (0.355 mmol) of solid *cis*-$[Pt(DMSO)_2Cl_2]$, which resulted in immediate formation of a brick-red suspension. The mixture was allowed to stir for 3 h and then filtered to separate the product. The red solid was filtered and washed several times with MeCN and then with diethyl ether (Et_2O) to remove any unreacted ligand and excess base. Yield: 158 mg (80%) crude product, 80% pure by NMR. The product can be purified further by vapor diffusion of Et_2O into a methanol (MeOH) solution, but a great deal of compound is lost in the process (27% yield). ^1H NMR (400 MHz, DMSO-d_6, 25 °C, 1.1 mM): δ 9.27 (d, 2H), 8.68 (d, 2H), 8.17 (d, 2H), 8.02 (d, 2 H), 7.74 (dd, 2H), 7.66–7.60 (m, 4H), 5.51 (t, 1H). IR (KBr, cm^{-1}): 3433 s, 3031 vw, 2967 vw, 2919 vw, 2846 vw, 2381 w, 2349 w, 2310 vw, 1631 w, 1583 m, 1496 s, 1466 vs, 1399 m, 1384 m, 1357 w, 1331 w, 1313 s, 1279 m, 1214 w, 1134 w, 1089 w, 821 m, 803 w, 759 m, 626 vw, 581 vw, 563 vw, 531 w, 476 w. ESI-MS (pos. ion mode, MeOH): *m*/*z* 517.9 (calcd. for $[Pt(BDI^{QQ})]$: 518.1). Anal. Calcd. for $[Pt(BDI^{QQ})]Cl\cdot 2H_2O$, $C_{21}H_{19}ClN_4O_2Pt$: C, 42.75; H, 3.25; N, 9.50. Found: C, 43.03; H, 2.94; N, 9.39

Synthesis of $[Pt(BDI^{QQ})]Cl\cdot 2H_2O$ from *cis*/*trans*-$[Pt(SMe_2)_2Cl_2]$. To a yellow solution of *cis/trans*-$[Pt(SMe_2)Cl_2]$ (100 mg, 0.26 mmol) in 8 mL of MeCN was added dropwise a mixture of TEA (90 mg, 0.89 mmol) and $BDI^{QQ}H\cdot 3HCl$ (120 mg, 0.26 mmol) in 5 mL MeCN. After stirring for 12 h at room temperature, the resulting brick-red solid was collected by filtration and washed with 3 × 5 mL MeCN and 3 × 5 mL Et_2O. The solid was then dissolved in 30 mL of boiling methanol. The resulting solution was filtered while still hot. The slow vapor diffusion of Et_2O into this solution over the course of three days at room temperature afforded dark purple needle-like crystals of the desired product. These crystals were collected by filtration, washed with 3 × 5 mL Et_2O, and then dried in vacuo. Yield: 54 mg (35%). Anal. Calcd. for

[Pt(BDI^{QQ})]Cl·2H$_2$O, $C_{21}H_{19}ClN_4O_2Pt$: C, 42.75; H, 3.25; N, 9.50. Found: C, 43.52; H, 3.09; N, 9.47. Other spectroscopic data matched those described above.

DFT Calculations. The ORCA software package[6] was utilized for DFT calculations. Starting from the coordinates obtained from the X-ray crystal structure, the geometry of [Pt(BDI^{QQ})]$^+$ was optimized in the gas phase as a singlet at the BP86 level of theory[7-9] using the def2-TZVP(-f) and def2-TZVP/j basis and auxiliary basis sets with the zeroth-order regular approximation (ZORA) to account for relativistic effects.[10,11] The optimized geometry was a local minimum on the potential energy surface as evidenced by a frequency calculation at the same level of theory, which gave rise to only real values. The optimized geometry was used for subsequent time-dependent DFT (TDDFT) calculations. For these calculations, the COSMO solvation model[12] for DMSO was applied, and the hybrid B3LYP functional[13,14] was used; the relativistic basis sets used for the geometry optimization were retained. The 20 lowest energy singlet and triplet excited states were computed. These excited states were visualized by electron-density difference maps (EDDMs), which depict the electron redistribution relative to the ground state. An additional geometry optimization of [Pt(BDI^{QQ})]$^+$ as a triplet was carried out using the same functional and basis sets for the singlet. Likewise, a frequency calculation revealed the optimized triplet geometry to be a minimum on the potential energy surface. A single-point calculation on the triplet with the B3LYP functional and COSMO solvation model was undertaken to determine the energy of the optimized triplet state relative to that of the singlet. Thermal and zero-point energy corrections, obtained from the frequency calculations at the BP86 level of theory, were applied to the higher level single-point calculations.

X-Ray Crystallography. A crystal of [Pt(BDI^{QQ})]Cl, grown by the vapor diffusion of Et_2O into a DMF solution, was mounted in Paratone oil on a cryoloop and frozen under a 100 K KRYOFLEX nitrogen stream. Data were obtained using a Bruker APEX CCD X-ray diffractometer with graphite-monochromated Mo Kα radiation (λ=0.71073 Å) controlled by the *APEX2* software.[15] From the diffraction pattern of the selected crystal, signs of non-merohedral twinning in the form of split reflections were observed. Accordingly, after a full data collection, two independent orientations of two twin domains were located with the program *CELL_NOW*.[16] A minor domain, oriented approximately 180° about *a** axis, was located. The data were integrated over both domains with *SAINT*,[17] and an absorption correction was applied with *TWINABS*.[18] After determination of the space group with *XPREP*,[19] the integrated data were solved and refined using the *Olex2* suite of programs.[20] Only data from the major domain was used for refinement. All components of the cation, [Pt(BDI^{QQ})]$^+$, were located on the difference map and refined satisfactorily. These planar cations packed efficiently in columns that propagated down the crystallographic *b*-axis. Large solvent accessible voids with diffuse electron density remained in the structure. After full assignment of the atoms of the [Pt(BDI^{QQ})]$^+$ cation, the largest residual electron density peak (19 e^- before adjustment of the weighting scheme) was assigned to be the chloride counterion. Still, additional significant residual electron density remained that could not be satisfactorily modeled as discrete solvent molecules. To account for this diffuse electron density, the solvent masking protocol of *Olex2* was employed. Four symmetry-related solvent accessible voids in the unit cell were each found to have a volume of 309 Å^3 and contain density corresponding to 133 electrons. This density is tentatively assigned to 3.2 molecules of diethyl ether, which totals to 134 electrons. This assignment corresponds to a reasonable non-H atomic volume of 19 electron per atom for the disordered solvent The largest residual electron peak and hole are 3.97 and -5.38 e·Å^{-3}, both located less than 2 Å from the Pt center. These large values may arise from an imperfect absorption correction or a Fourier truncation error. Data collection and refinement parameters for the final model are presented in Table S1.

DNA-Binding Studies. Ultra-pure calf-thymus DNA (CT-DNA) was purchased from Invitrogen. To a 5 μM solution of the platinum complex in 10 mM pH 7.4 Tris buffer supplemented with 10 mM NaCl, were added aliquots of CT-DNA. The equilibration time, when no further changes in the absorbance or emission spectra were observed, was approximately 2 h. Because of this long equilibration time, 14–16 samples with different DNA:Pt ratios ranging from 0–500 were prepared and incubated overnight in the dark at room temperature. The absorbance and emission spectra of these samples were measured and the maxima were plotted against the DNA concentration . The data were fit to the equation, $(A_o - A_f)/(A_b - A_f) = K[DNA]/(1+K[DNA])$ where A_o is the measured absorbance or emission, A_f is the absorbance or emission of the platinum complex in the absence of DNA, A_b is the absorbance or emission of the platinum complex fully bound to DNA, K is the binding constant, and [DNA] is the concentration of DNA in nucleotides. This equation is valid for weak, 1:1 DNA-binding molecules where the [DNA] is > 10 times that of the complex of interest for all data points, as is the case here.[25] The temperature was controlled at 25 °C, and samples were excited at 540 nm. Fitting the emission data in a similar fashion gave comparable binding constants. This experiment was repeated three times and the reported binding constant is the average of three trials of both the UV-vis and emission data where the reported error is the standard deviation.

Cytotoxicity Measurements. Human HeLa (cervical cancer) and A549 (lung carcinoma) were grown as adherent monolayers in Dulbecco's Modified Eagle Medium (DMEM) supplemented with 10% fetal bovine serum and 1% penicillin/streptomycin. The cultures were grown in 25 cm^2 flasks in an incubator at 37 °C with a humidified atmosphere including 5% CO_2.

The cytotoxicity of cisplatin and $[Pt(BDI^{QQ})]Cl$ were determined by the colorimetric MTT assay. Cisplatin was diluted from a PBS solution. Because of the low solubility of $[Pt(BDI^{QQ})]Cl$ in aqueous media, a concentrated solution was first prepared in DMSO and then diluted such that the highest dose given to cells contained only 1% DMSO. Parallel assays, investigating the toxicity of DMSO alone, were also run. The data from these additional assays were used to correct for the effect of DMSO on the measured toxicity of $[Pt(BDI^{QQ})]Cl$.

Trypsinized HeLa and A549 cells were seeded into 96-well plates at a cell density of 2000 cells/well in 200 μL of growth medium and were incubated for 24 h. The wells were then aspirated and 200 μL of new media containing various concentrations of the platinum complexes were added to each well. After a 72-h incubation period, the medium was aspirated again, and a 0.8 mg/mL solution of MTT in DMEM was added. The plate was incubated for another 4 h, aspirated, and then a 200 μL solution of 4% ammonia in DMSO was added to each well to dissolve the purple formazan crystals. The absorbance of the plates was read at 550 nm. Absorbance values were normalized to platinum-free control wells and plotted as [Pt] versus per cent viability. IC_{50} values were interpolated from the resulting curves, and the reported values are the averages from three independent trials for HeLa and 2 independent trials for A549, each of which consisted of six replicates per concentration level.

Table S1. X-ray Crystallographic Data Collection and Refinement Parameters for $[Pt(BDI^{QQ})]^+$.

formula	$C_{21}H_{15}ClN_4Pt$	ρ_{calcd}, g·cm^{-3}	1.6756
fw	553.91	T, °C	-173(2)
space group	$C2/c$	μ(Mo Kα), mm^{-1}	6.400
a, Å	28.326(4)	Θ range, deg	1.61 to 28.35
b, Å	6.7809(9)	completeness to Θ (%)	99.7
c, Å	25.610(4)	total no. of data	68863
β, deg	116.790(2)	no. of unique data	5457
V, Å^3	4391.2(11)	no. of parameters	243
Z	8	R1[a] (%)	5.30
crystal size, mm	0.25 × 0.08 × 0.04	wR2[b] (%)	12.77
color	dark purple	GOF[c]	1.016
habit	needle	max, min peaks, e· Å^{-3}	3.97, -5.38

[a] $R1 = \Sigma||F_o| - |F_c||/\Sigma|F_o|$. [b] $wR2 = \{\Sigma[w(F_o^2 - F_c^2)^2]/\Sigma[w(F_o^2)^2]\}^{1/2}$. [c] $GOF = \{\Sigma[w(F_o^2 - F_c^2)^2]/(n - p)\}^{1/2}$ where n is the number of data and p is the number of refined parameters.

Table S2. Interatomic Distances (Å) and Angles (°) for $[Pt(BDI^{QQ})]^+$.[a]

Bonds		Angles			
Pt1–N1	2.049(6)	N1–Pt1–N2	80.6(2)	N2–Pt1–N4	173.2(2)
Pt1–N2	1.990(5)	N1–Pt1–N3	173.7(2)	N3–Pt1–N4	80.7(2)
Pt1–N3	2.000(5)	N1–Pt1–N4	104.7(2)		
Pt1–N4	2.039(5)	N2–Pt1–N3	94.1(2)		

[a] Numbers in parentheses are the estimated standard deviations in the last significant figures. Atoms are labeled as indicated in Figure 1 of the main text.

Table S3. Cartesian Coordinates (Å) for the DFT-Optimized Structure of Singlet $[Pt(BDI^{QQ})]^+$.

Pt	-0.269714	-0.002398	-0.045446
N	-2.253457	-0.063866	-0.261855
N	-0.310988	-0.013238	1.950453
N	-0.392591	0.219141	-2.084081
C	-2.701350	-0.113768	-1.595030
C	3.388221	-0.075423	2.151700
C	-1.679493	0.071902	-2.561785
C	-4.006571	-0.302424	-2.037753
H	-4.819694	-0.470122	-1.332907
C	-4.305139	-0.279648	-3.416495
H	-5.337857	-0.434952	-3.729641
C	0.950867	0.070564	2.567845
C	3.617240	0.086585	3.541650
H	4.639817	0.076982	3.919567
C	2.739622	-0.422184	-0.518121
H	2.463910	-0.599449	-1.554954
C	0.566472	0.553640	-2.952064
H	1.552371	0.753303	-2.539052
C	1.215298	0.227820	3.924518
H	0.406101	0.339897	4.644750
C	-3.094638	-0.104498	0.774565
H	-4.161722	-0.143637	0.546222
C	4.416690	-0.298018	1.204840
H	5.456230	-0.331667	1.534625
C	-1.446991	-0.046761	2.651778
H	-1.358424	-0.044244	3.740125
C	-3.326344	-0.050018	-4.363417
H	-3.570839	-0.010037	-5.425133

C	-2.735854	-0.093461	2.121895
H	-3.552997	-0.124379	2.840035
C	2.544577	0.245058	4.397148
H	2.716963	0.373979	5.465953
C	4.085324	-0.499609	-0.119156
H	4.844775	-0.713681	-0.869921
C	0.339566	0.673307	-4.334181
H	1.172397	0.942867	-4.982237
C	-1.983944	0.146963	-3.951313
C	-0.922910	0.442774	-4.840467
H	-1.118757	0.508781	-5.911832
N	1.743656	-0.155970	0.331698
C	2.046920	-0.040278	1.673528

Table S4. Cartesian Coordinates (Å) for the DFT-Optimized Structure of Triplet [Pt(BDI^{QQ})]$^{+}$.

Pt	-0.269982	-0.003449	-0.045624
N	-2.256900	-0.059076	-0.266064
N	-0.307056	-0.019384	1.953991
N	-0.375830	0.238385	-2.075090
C	-2.684520	-0.121852	-1.581305
C	3.378117	-0.077981	2.125427
C	-1.655398	0.074828	-2.549622
C	-4.007865	-0.321809	-2.024049
H	-4.814455	-0.501902	-1.316458
C	-4.294343	-0.301421	-3.393021
H	-5.321756	-0.466553	-3.718244
C	0.939026	0.079174	2.549236
C	3.597311	0.099421	3.518427
H	4.618887	0.090792	3.899287
C	2.731830	-0.474293	-0.546260
H	2.444327	-0.676946	-1.574847
C	0.591746	0.604072	-2.938583
H	1.567194	0.827125	-2.513785
C	1.200675	0.248312	3.924105
H	0.389108	0.373039	4.637917
C	-3.117207	-0.116949	0.776210
H	-4.180790	-0.168580	0.550287
C	4.405045	-0.316929	1.180422
H	5.444392	-0.351186	1.509030
C	-1.451783	-0.037920	2.674405
H	-1.365586	-0.023282	3.759445
C	-3.305910	-0.059993	-4.341118

H	-3.553462	-0.020207	-5.402199
C	-2.732681	-0.094930	2.119233
H	-3.551343	-0.126195	2.838831
C	2.521704	0.269521	4.383565
H	2.706247	0.410173	5.448827
C	4.069556	-0.544379	-0.144734
H	4.829817	-0.779677	-0.888292
C	0.361684	0.717123	-4.313298
H	1.187021	1.007077	-4.962137
C	-1.959575	0.151380	-3.937803
C	-0.900817	0.462770	-4.824857
H	-1.095393	0.530325	-5.895817
N	1.737674	-0.176349	0.313013
C	2.038033	-0.042439	1.647599

Table S5. Summary of 20 Lowest Energy Singlet Excited States of $[Pt(BDI^{QQ})]^+$ in DMSO Computed by TDDFT.

No.	**Energy (cm^{-1})**	**Wavelength (nm)**	**Osc. Strength**	**Major Contribs**
1	18568.5	538.5	0.166869898	HOMO → LUMO (94%)
2	18722.1	534.1	0.000157566	HOMO → LUMO+1 (97%)
3	26660.7	375.1	0.049595986	HOMO-1 → LUMO (87%)
4	26464.0	377.9	0.028186776	HOMO-1 → LUMO+1 (82%) HOMO → LUMO+2 (11%)
5	25305.1	395.2	0.001066443	HOMO-3 → LUMO (97%)
6	28772.2	347.6	0.024795193	HOMO-2 → LUMO (43%) HOMO → LUMO+2 (48%)
7	30114.5	332.1	0.519075783	HOMO-2 → LUMO (47%) HOMO-1 → LUMO+1 (13%) HOMO → LUMO+2 (30%)
8	27255.0	366.9	0.017302173	HOMO-3 → LUMO+1 (96%)
9	30193.1	331.2	0.000027483	HOMO-4 → LUMO (11%) HOMO → LUMO+3 (78%)

10	30650.4	326.3	0.011720277	HOMO-5 → LUMO (12%) HOMO → LUMO+4 (82%)
11	31424.4	318.2	001664276	HOMO → LUMO+5 (88%)
12	31554.1	316.9	0.013657172	HOMO-2 → LUMO+1 (85%)
13	32549.9	307.2	0.022210227	HOMO-6 → LUMO (18%) HOMO-4 → LUMO (63%)
14	34230.8	292.1	0.056004082	HOMO-5 → LUMO (53%) HOMO-1 → LUMO+3 (22%) HOMO → LUMO+4 (13%)
15	35010.3	285.6	0.023889805	HOMO-6 → LUMO (51%) HOMO-1 → LUMO+4 (24%)
16	35021.7	285.5	0.051453169	HOMO-5 → LUMO (12%) HOMO-4 → LUMO+1 (73%)
17	35504.4	281.7	0.004603948	HOMO-6 → LUMO (11%) HOMO-5 → LUMO+1 (12%) HOMO-1 → LUMO+2 (61%)
18	36154.7	276.6	0.000510518	HOMO-5 → LUMO+1 (51%) HOMO-1 → LUMO+2 (14%) HOMO-1 → LUMO+4 (12%)
19	36325.9	275.3	0.011680578	HOMO-6 → LUMO+1 (63%) HOMO-1 → LUMO+3 (19%)
20	35161.0	284.4	0.002044896	HOMO-3 → LUMO+2 (87%)

Table S6. Summary of 20 Lowest Energy Triplet Excited States of $[Pt(BDI^{QQ})]^+$ in DMSO Computed by TDDFT.

No.	Energy (cm^{-1})	Wavelength (nm)	Osc. Strength	Major Contribs
1	14841.3	673.8	0	HOMO → LUMO (92%)
2	18248.3	548.0	0	HOMO-1 → LUMO (28%) HOMO → LUMO+1 (66%)
3	21207.5	471.5	0	HOMO-1 → LUMO (60%) HOMO → LUMO+1 (32%)
4	22155.8	451.3	0	HOMO-2 → LUMO (23%) HOMO-1 → LUMO+1 (57%) HOMO → LUMO+2 (12%)
5	25242.6	396.2	0	HOMO → LUMO+2 (77%)
6	26993.9	370.5	0	HOMO-2 → LUMO+1 (50%) HOMO-1 → LUMO+2 (23%)
7	27976.7	357.4	0	HOMO-2 → LUMO (56%) HOMO-1 → LUMO+1 (21%)
8	28257.5	353.9	0	HOMO-5 → LUMO+1 (13%)

				HOMO-3 → LUMO (48%)
9	28497.4	350.9	0	HOMO-5 → LUMO (37%) HOMO-4 → LUMO+1 (13%) HOMO-2 → LUMO (11%) HOMO → LUMO+4 (13%)
10	28532.4	350.5	0	HOMO-3 → LUMO (35%) HOMO → LUMO+3 (27%) HOMO → LUMO+5 (21%)
11	28904.5	346.0	0	HOMO-5 → LUMO+1 (15%) HOMO-4 → LUMO (20%) HOMO → LUMO+5 (34%)
12	29221.2	342.2	0	HOMO-4 → LUMO (11%) HOMO → LUMO+3 (51%) HOMO → LUMO+5 (17%)
13	29433.4	339.7	0	HOMO → LUMO+4 (72%)
14	30360.6	329.4	0	HOMO-3 → LUMO+1 (87%)
15	31336.3	319.1	0	HOMO-6 → LUMO (35%) HOMO-4 → LUMO (11%) HOMO-1 → LUMO+2 (27%)
16	32089.3	311.6	0	HOMO-6 → LUMO (16%) HOMO-4 → LUMO (16%) HOMO-2 → LUMO+1 (24%) HOMO-1 → LUMO+2 (31%)
17	32753.6	305.3	0	HOMO-7 → LUMO (19%) HOMO-6 → LUMO+1 (17%) HOMO-4 → LUMO+1 (20%)

				HOMO-1 → LUMO+5 (13%)
18	33971.5	294.4	0	HOMO-6 → LUMO+5 (13%) HOMO-3 → LUMO+5 (14%) HOMO-1 → LUMO+5 (38%)
19	34414.9	290.6	0	HOMO-3 → LUMO+5 (71%)
20	34856.5	286.9	0	HOMO-7 → LUMO (14%) HOMO-2 → LUMO+2 (13%) HOMO-1 → LUMO+3 (32%)

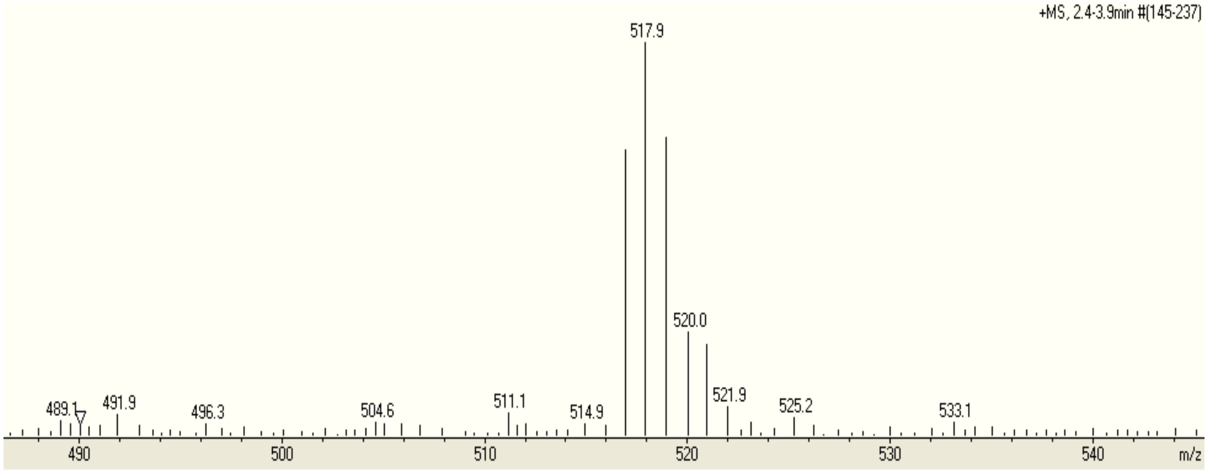

Fig. S1. ESI-MS of [Pt(BDI^{QQ})]Cl in the positive ion mode. *m*/*z* calc. for [Pt(BDI^{QQ})]$^{+}$ is 518.1.

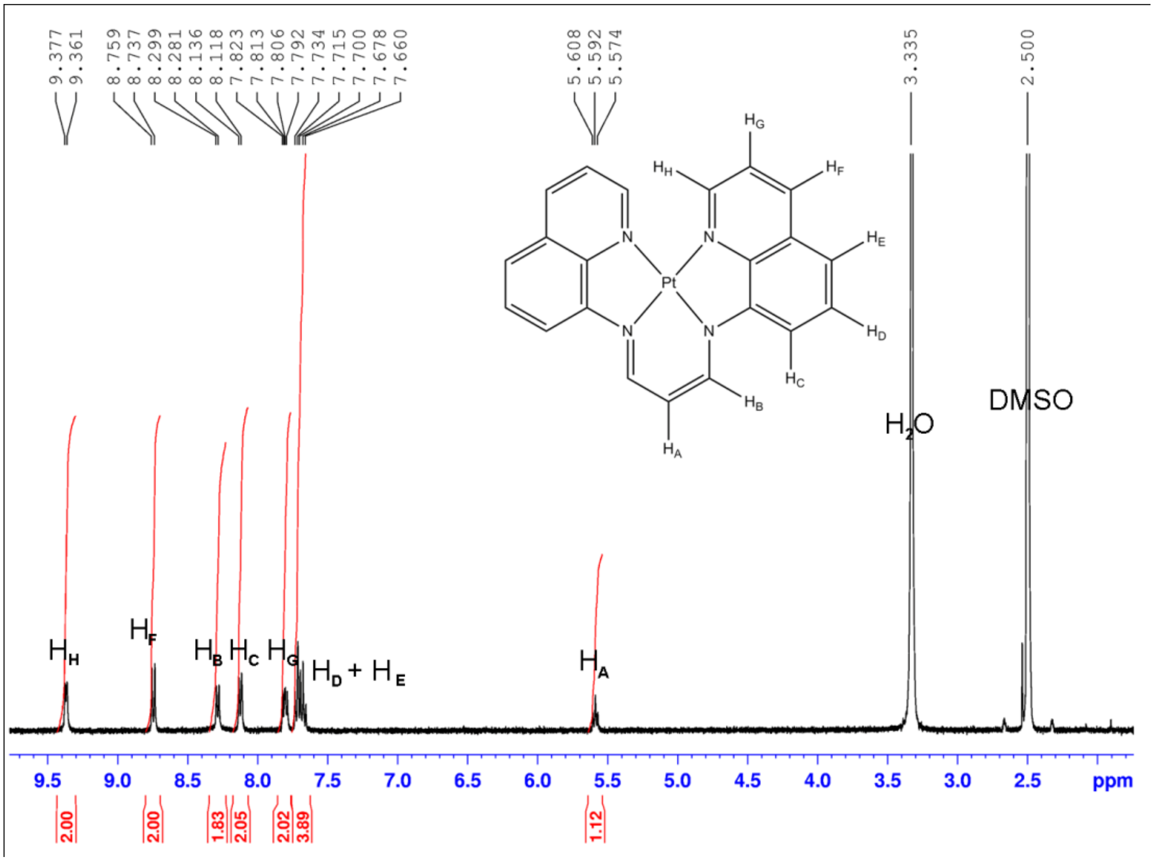

Fig. S2. ^{1}H NMR spectrum of the $[Pt(BDI^{QQ})]^+$ cation recorded in DMSO-d_6.

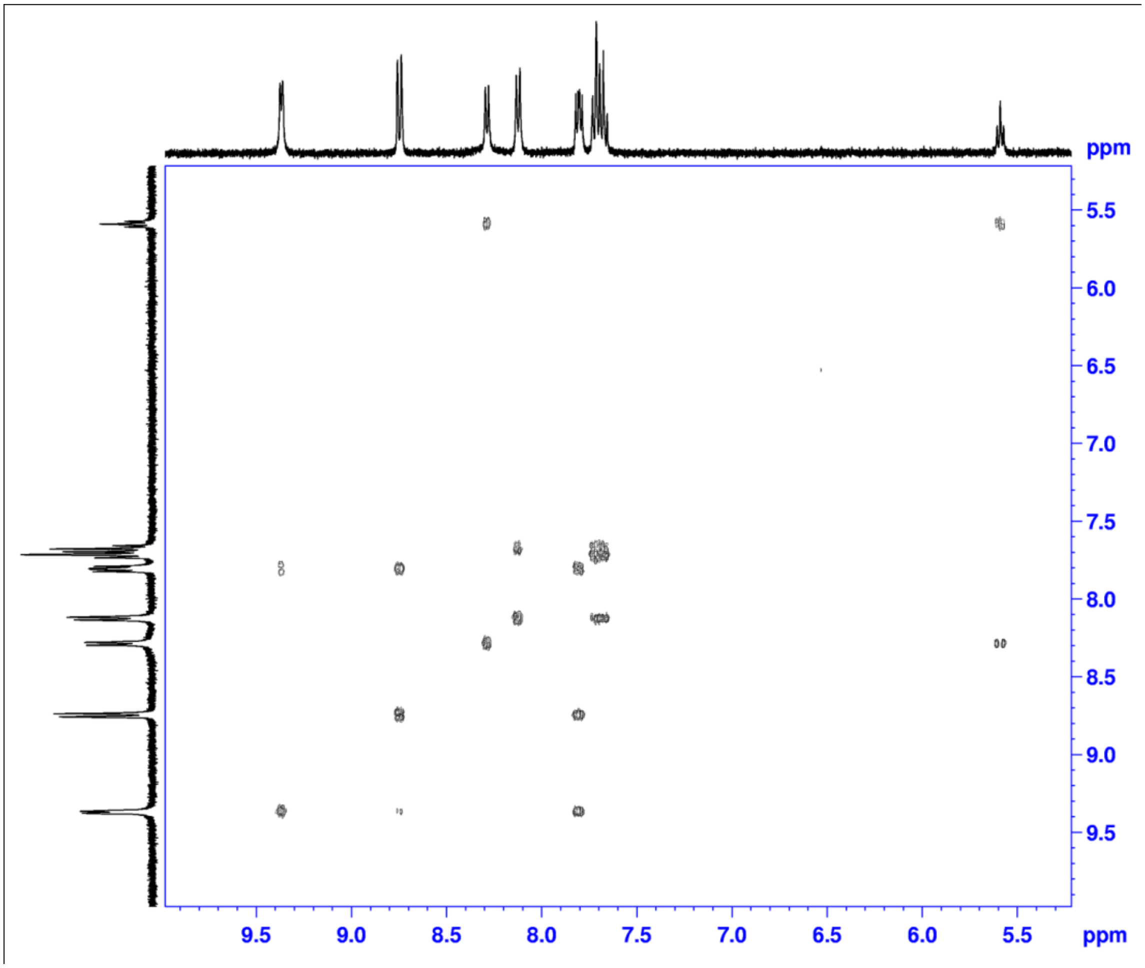

Fig. S3. 2-D COSY NMR spectrum of the [Pt(BDI^{QQ})]$^+$ cation recorded in DMSO-d_6.

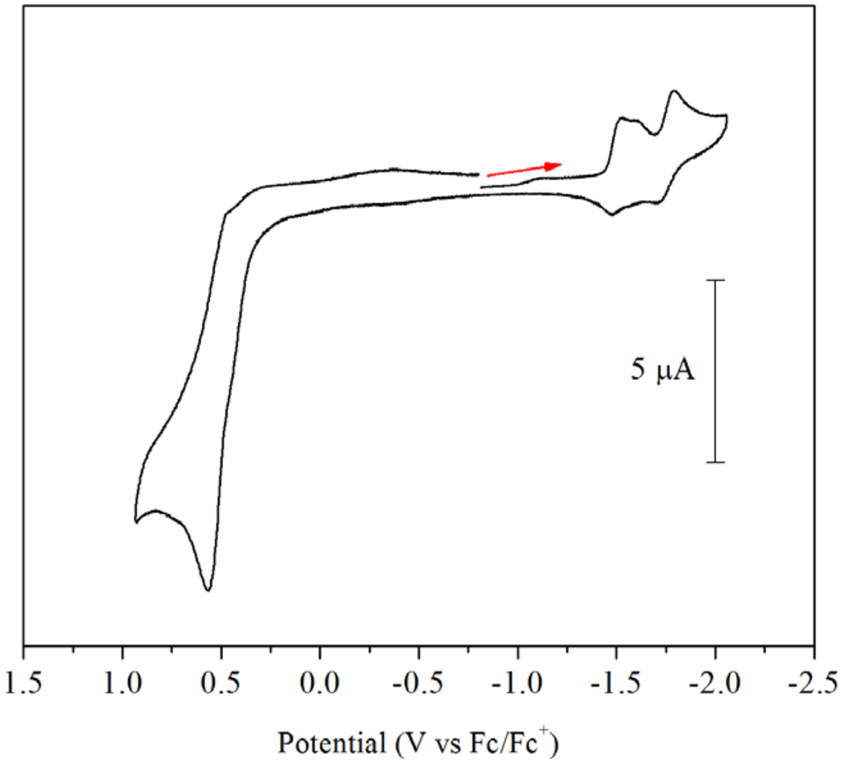

Fig. S4. Cyclic voltammogram of [Pt(BDI^{QQ})]Cl recorded in DMF with 0.1 M $Bu_4N(PF_6)$ at a scan rate of 20 mV/s. The red arrow marks the starting potential and initial scan direction.

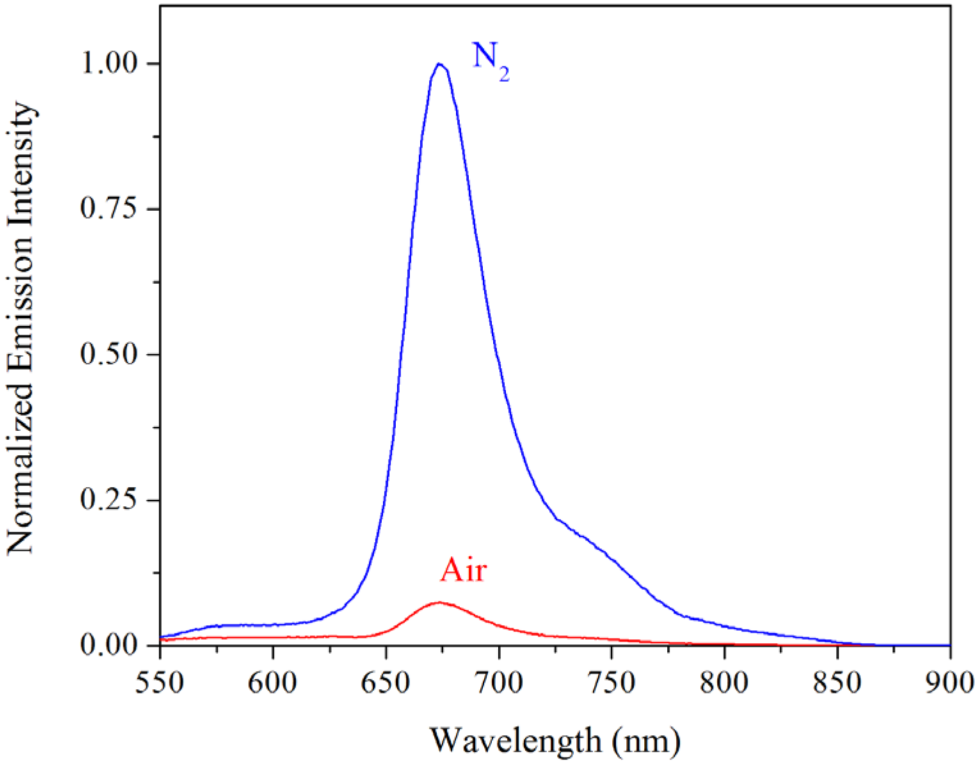

Fig. S5. Emission spectra of [Pt(BDI^{QQ})]Cl (5 μM) in air-equilibrated (red) or N_2-purged (blue) DMSO, excited at 540 nm.

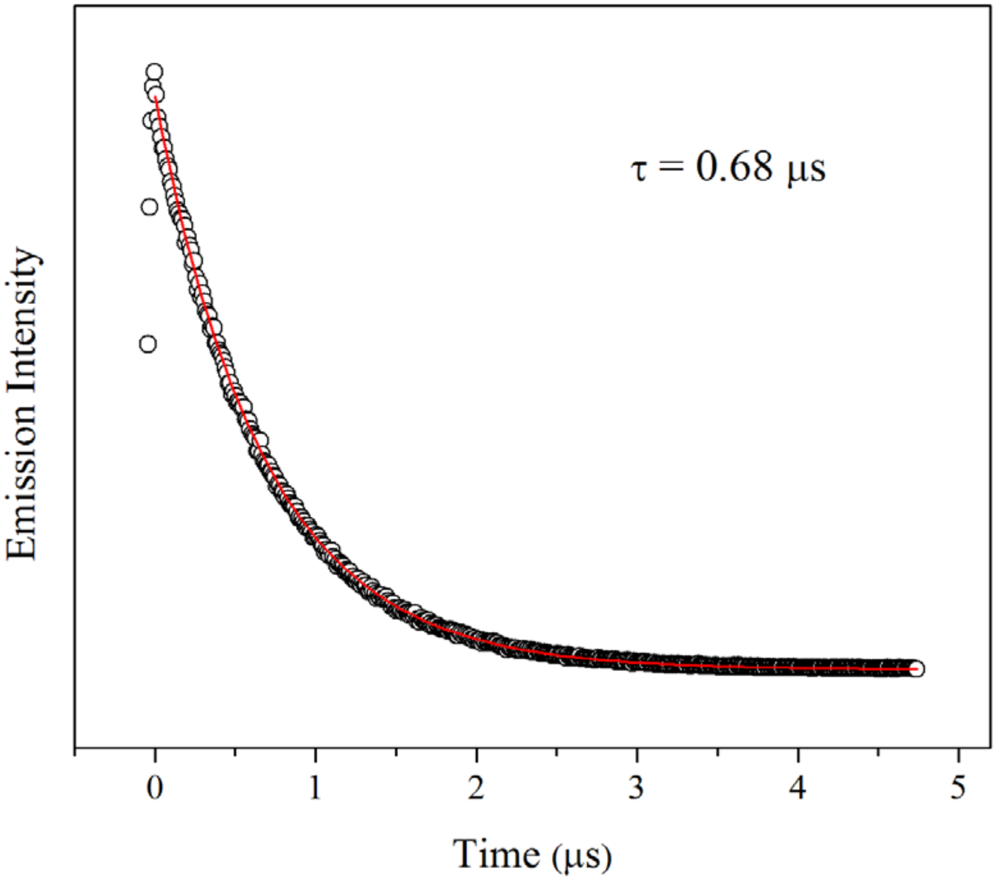

Fig. S6. Time-resolved emission decay profile of [Pt(BDI^{QQ})]Cl in air-equilibrated DMSO solution at 15 μM concentration excited at 550 nm.

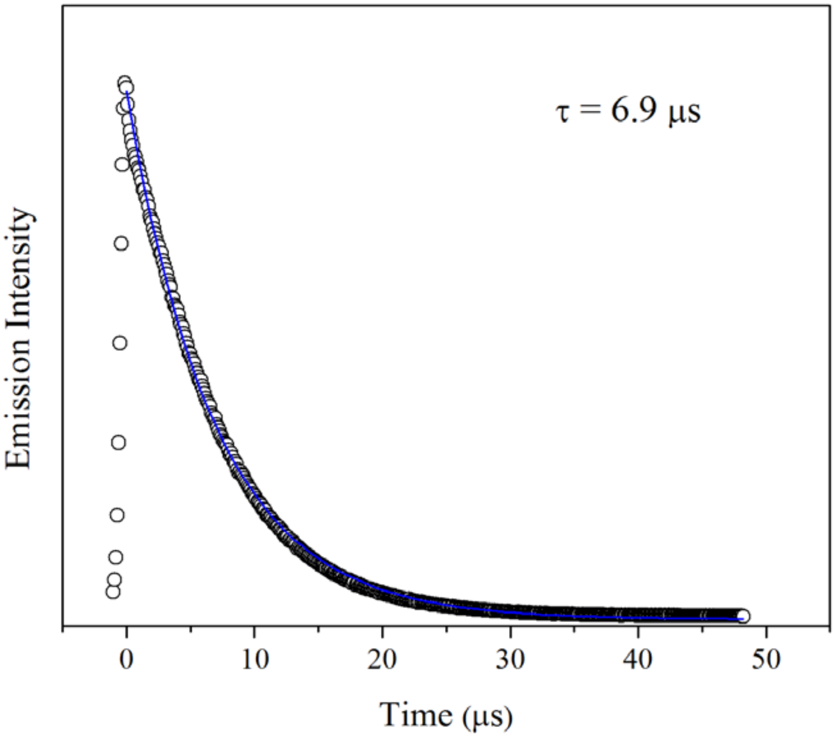

Fig. S7. Time-resolved emission decay profile of [Pt(BDI^{QQ})]Cl in N_2-purged DMSO solution at 15 μM concentration excited at 550 nm.

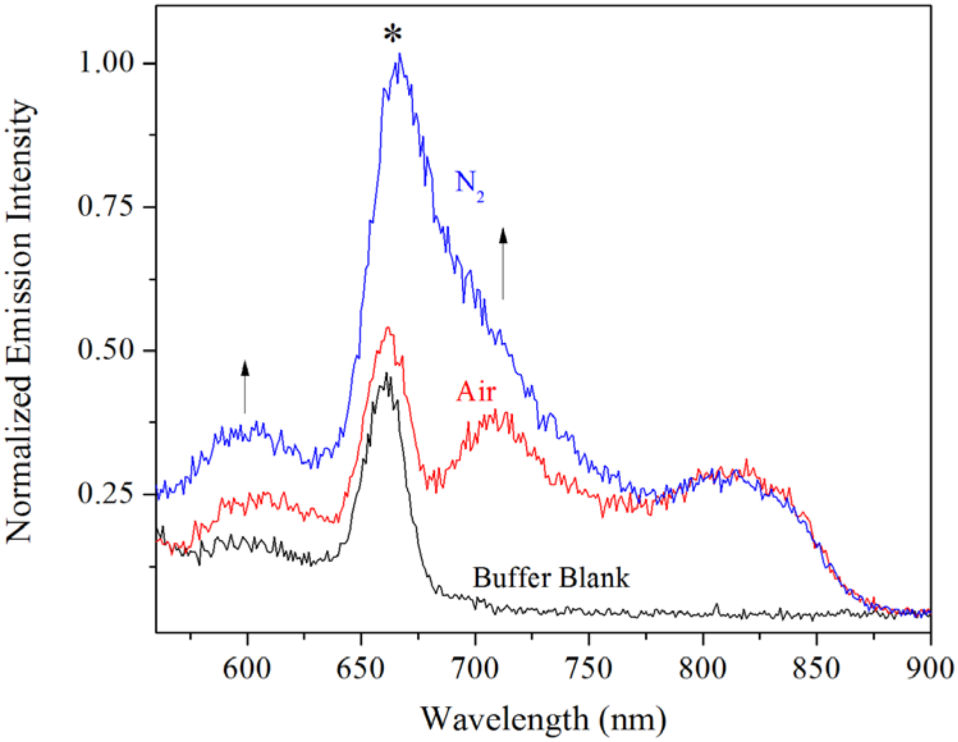

Fig. S8. Emission spectra of [Pt(BDI^{QQ})]Cl (5 μM) in aqueous buffer (pH 7.4, 10 mM Tris, 10 mM NaCl) under air (red) or N_2 (blue) atmosphere, excited at 540 nm. The feature at 660 nm appears in the blank and most likely arises from scattered excitation light.

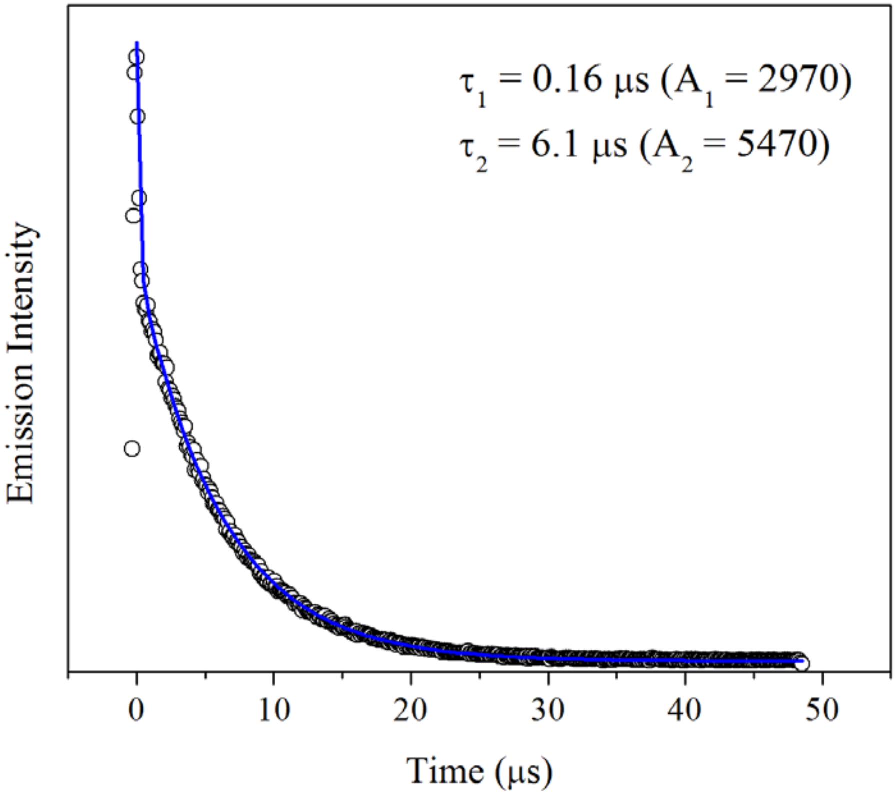

Fig. S9. Time-resolved emission decay profile of a 15 μM solution of [Pt(BDI^{QQ})]Cl in aqueous buffer (pH 7.4, 10 mM Tris, 10 mM NaCl) in the presence of 30 mM CT-DNA. The sample was excited at 550 nm.

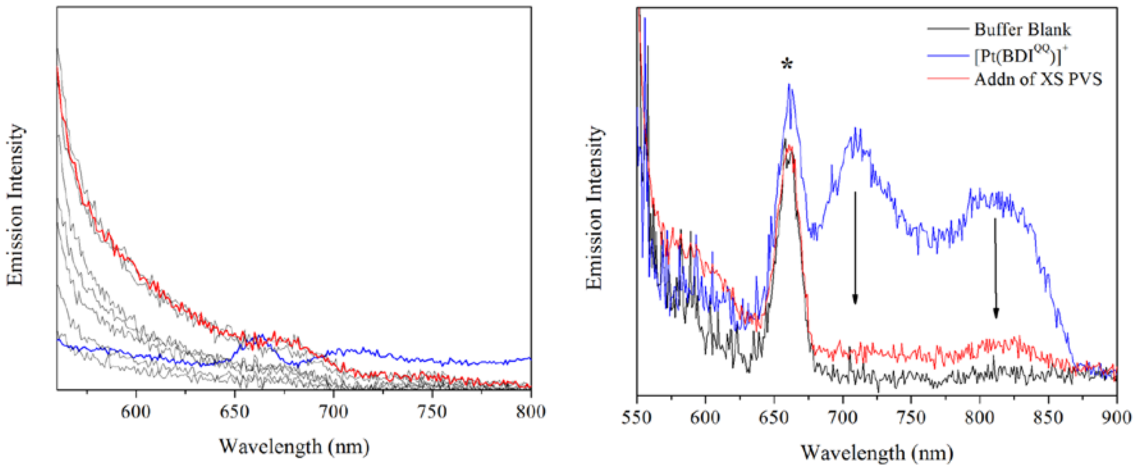

Fig. S10. Change in the emission spectra of $[Pt(BDI^{QQ})]Cl$ in aqueous buffer (pH 7.4, 10 mM Tris, 10 mM NaCl) upon the addition of a large excess of bovine serum albumin (left, blue before, red after) and polyvinyl sulfonic acid (right, blue before, red after).

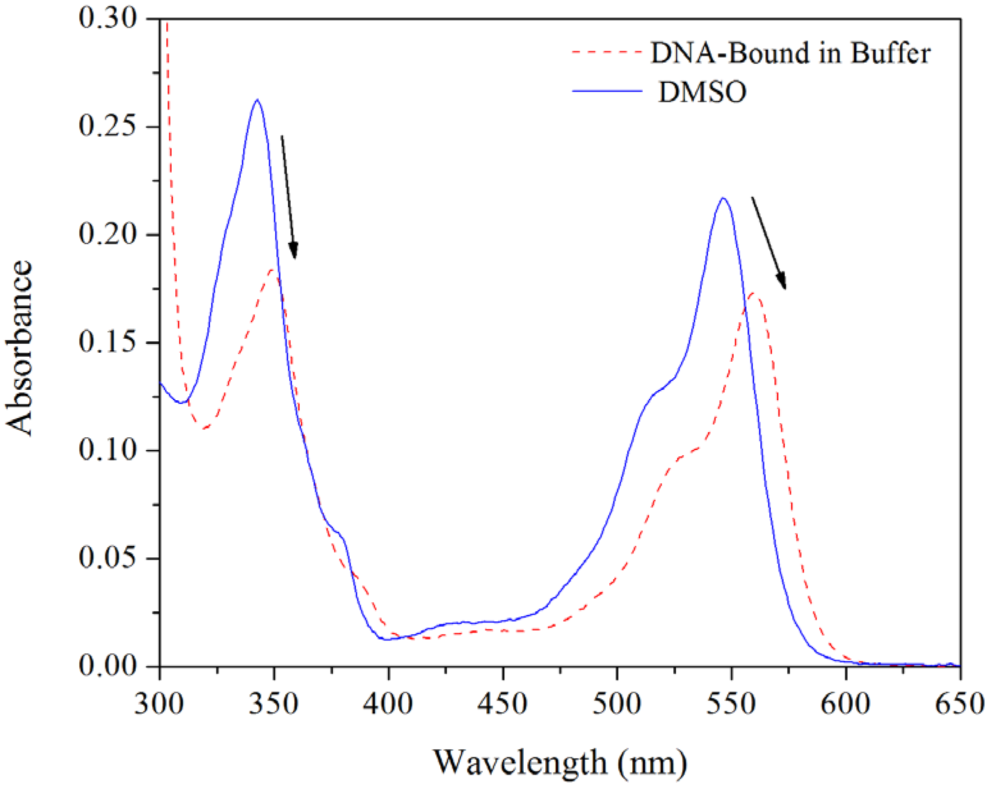

Fig. S11. Comparison of the UV-vis spectra of [Pt(BDI^{QQ})]Cl (5 μM) in DMSO (blue) and in buffer (red, pH 7.4, 10 mM Tris, 10 mM NaCl) in the presence of 500 equiv DNA.

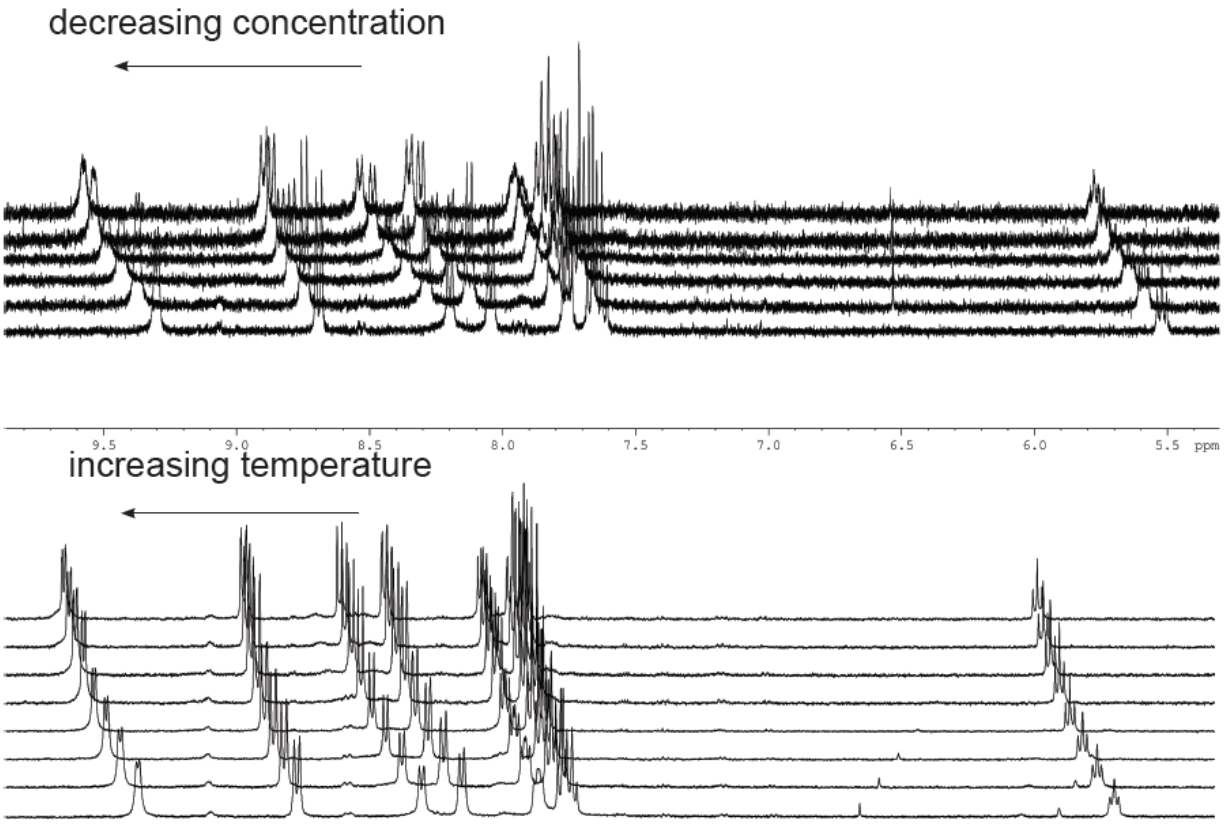

Fig. S12. The effect of concentration (top) and temperature (bottom) on the ^{1}H chemical shifts of [Pt(BDI^{QQ})]Cl in DMSO-d_6.

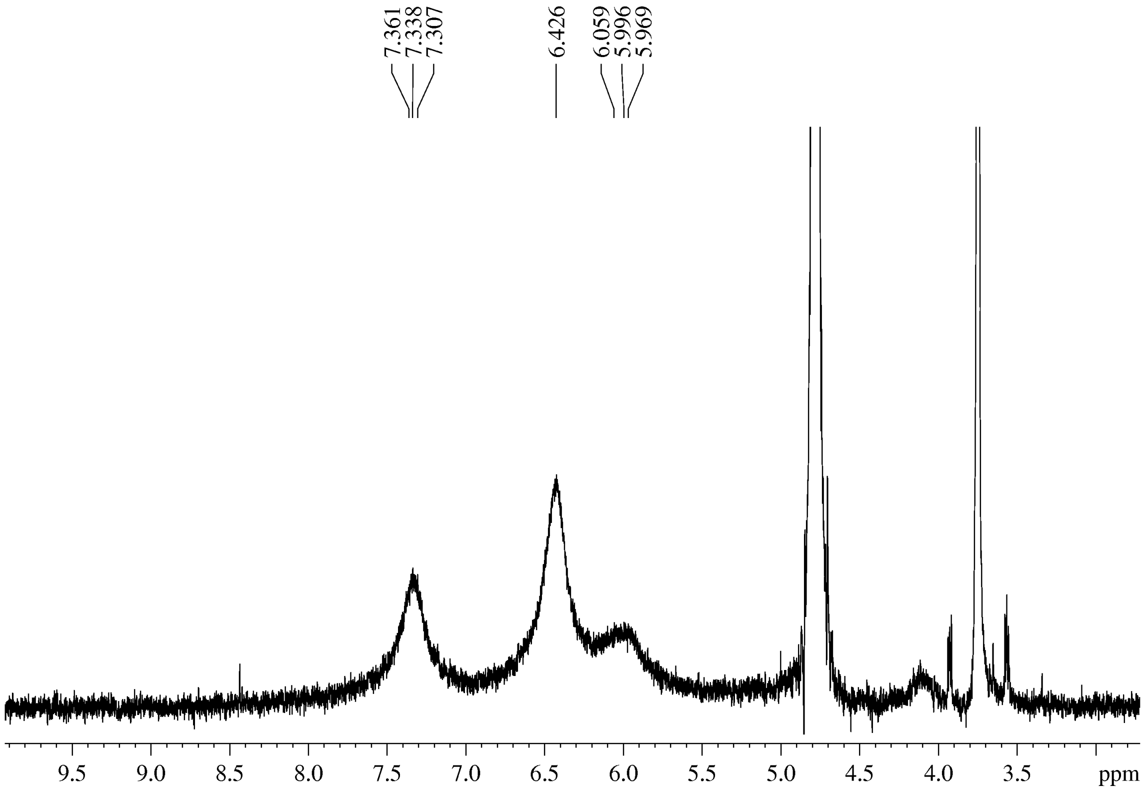

Fig. S13. ^{1}H NMR spectrum of [Pt(BDI^{QQ})]Cl (1.0 mM) in D_2O at 25 °C. The intense, sharp peaks near 4.8 and 3.75 ppm are HOD and 1,4-dioxane, added as an internal standard.

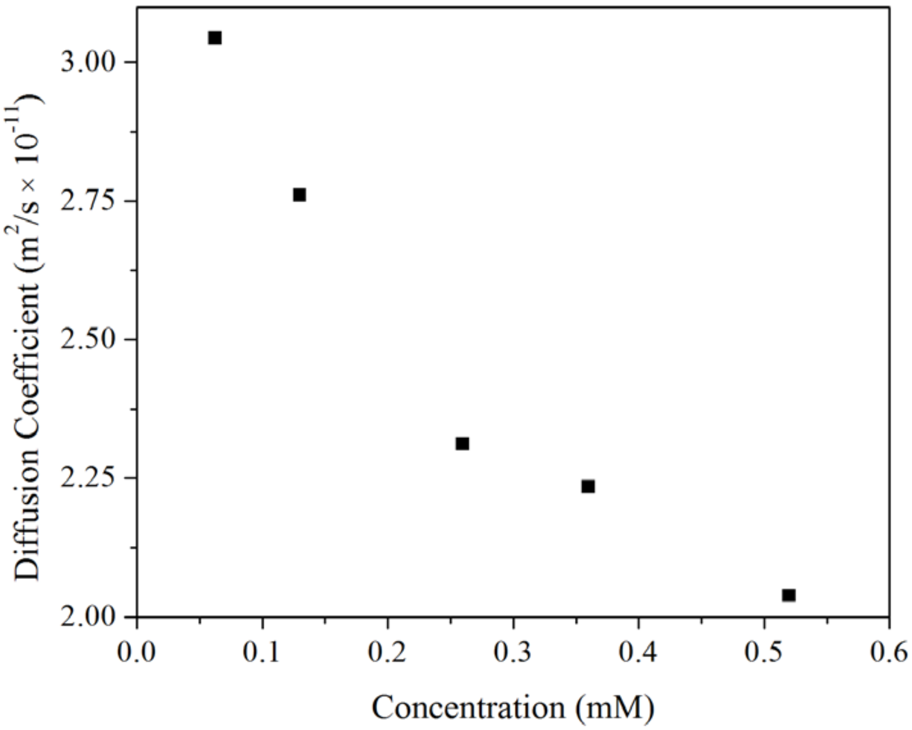

Fig. S14. Plot of concentration of [Pt(BDI^{QQ})]Cl in pH 7.4, 10 mM Tris, 10 mM NaCl versus average diffusion coefficient. The average diffusion coefficients were measured by dynamic light scattering (DLS).

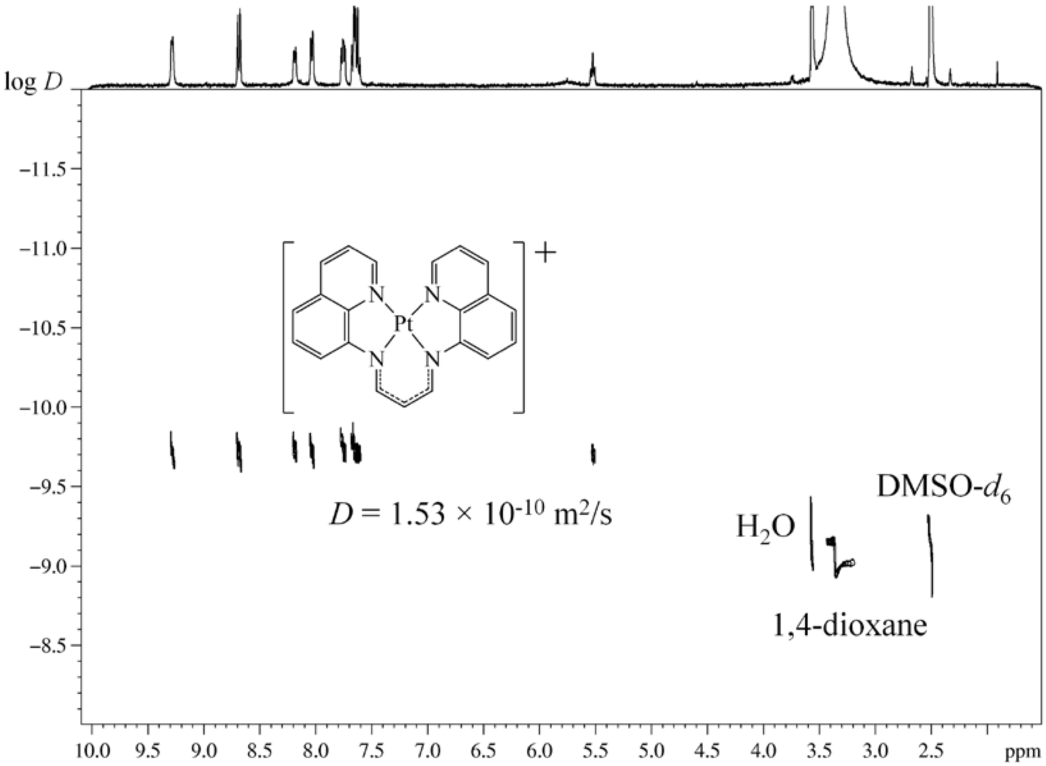

Fig. S15. 2-D DOSY NMR spectrum of [Pt(BDI^{QQ})]Cl (1.1 mM) in DMSO-d_6 at 25 °C.

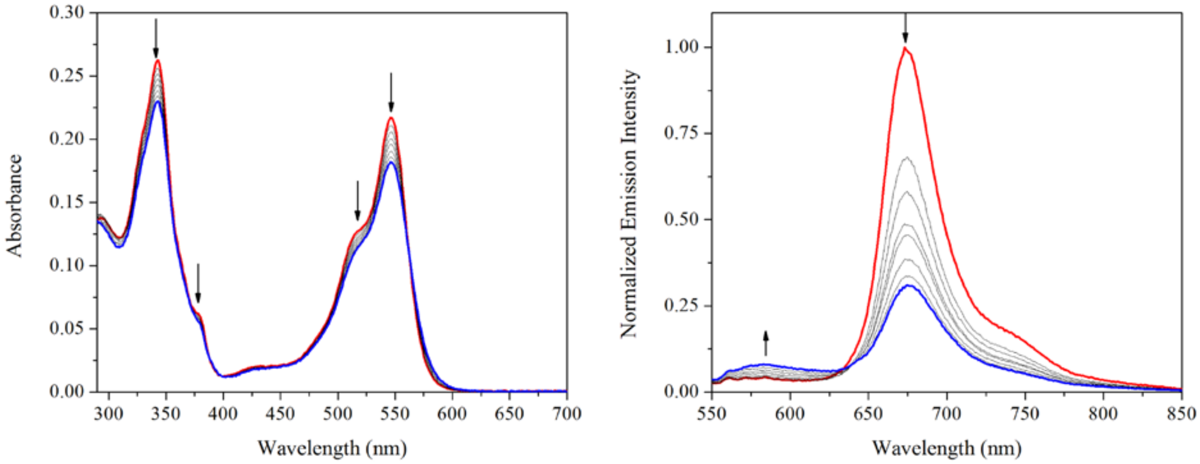

Fig. S16. UV-vis absorbance (left) and emission (right) spectra of [Pt(BDI^{QQ})]Cl (5 μM) in DMSO at varying temperatures from 20 °C (red) to 90 °C (blue) at 10 °C intervals. The black arrows mark the spectral changes as temperature increases.

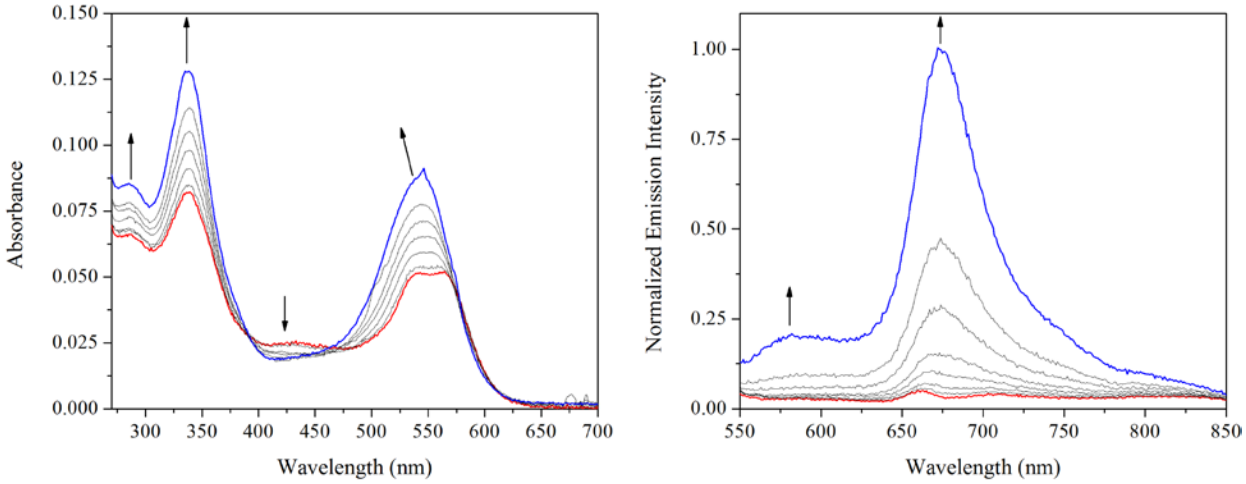

Fig. S17. UV-vis absorbance (left) and emission (right) spectra of $[Pt(BDI^{QQ})]Cl$ (5 μM) in aqueous buffer (pH 7.4, 10 mM Tris, 10 mM NaCl) at varying temperatures from 24 °C (red) to 94 °C (blue) at 10 °C intervals. The black arrows mark the spectral changes as temperature increases.

References:

(1) Zatka, V.; Holzbecher, J.; Ryan, D. E. *Anal. Chim. Acta* **1971**, *55*, 273-278.
(2) Kukushkin, V. Y.; Pombeiro, A. J. L.; Ferreira, C. M. P.; Elding, L. I.; Puddephatt, R. J. *Inorg. Synth.* **2002**, *33*, 189-196.
(3) Hill, G. S.; Irwin, M. J.; Levy, C. J.; Rendina, L. M.; Puddephatt, R. J.; Andersen, R. A.; McLean, L. *Inorg. Synth.* **2007**, *32*, 149-153.
(4) Suzuki, K.; Kobayashi, A.; Kaneko, S.; Takehira, K.; Yoshihara, T.; Ishida, H.; Shiina, Y.; Oishi, S.; Tobita, S. *Phys. Chem. Chem. Phys.* **2009**, *11*, 9850-9860.
(5) Damrauer, N. H.; Hodgkiss, J. M.; Rosenthal, J.; Nocera, D. G. *J. Phys. Chem. B* **2004**, *108*, 6315-6321.
(6) Neese, F. *ORCA, an Ab Initio, Density Functional and Semiempirical Electronic Structure Program Package*, Version 2.8; Universität Bonn: Bonn, Germany, 2010.
(7) Becke, A. D. *J. Chem. Phys.* **1986**, *84*, 4524-4529.
(8) Perdew, J. P.; Yue, W. *Phys. Rev. B* **1986**, *33*, 8800-8802.
(9) Perdew, J. P. *Phys. Rev. B* **1986**, *33*, 8822-8824.
(10) Weigend, F.; Ahlrichs, R. *Phys. Chem. Chem. Phys.* **2005**, *7*, 3297-3305.
(11) Pantazis, D. A.; Chen, X.-Y.; Landis, C. R.; Neese, F. *J. Chem. Theory Comput.* **2008**, *4*, 908-919.

(12) Klamt, A.; Schüürmann, G. *J. Chem. Soc.*, *Perkin Trans. 2* **1993**, 799-805.
(13) Becke, A. D. *J. Chem. Phys.* **1993**, *98*, 5648-5652.
(14) Lee, C.; Yang, W.; Parr, R. G. *Phys. Rev. B* **1988**, *37*, 785-789.
(15) *APEX2*, Version 2008-4.0; Bruker AXS, Inc.: Madison, WI, 2008.
(16) Sheldrick, G. M. *CELL_NOW*, University of Göttingen: Göttingen, Germany, 2008.
(17) *SAINT: SAX Area-Detector Integration Program*, Version 7.68; Bruker AXS, Inc.: Madison, WI, 2009.
(18) Sheldrick, G. M. *TWINABS*, University of Göttingen: Göttingen, Germany, 2008.
(19) *XPREP*, Version 2008/2; Bruker AXS, Inc.: Madison, WI, 2008.
(20) Dolomanov, O. V.; Bourhis, L. J.; Gildea, R. J.; Howard, J. A. K.; Puschmann, H. *J. Appl. Crystallogr.* **2009**, *42*, 339-341.
(21) Sheldrick, G. M. *SHELXTL-97*, Version 6.14; University of Göttingen: Göttingen, Germany, 2000.
(22) Sheldrick, G. M. *Acta Crystallogr. Sect. A* **2008**, *64*, 112-122.
(23) Spek, A. L. *J. Appl. Crystallogr.* **2003**, *36*, 7-13.
(24) Spek, A. L. *PLATON*, *A Multipurpose Crystallographic Tool*, Version 160312; Utrecht University: Utrecht, The Netherlands, 2012.
(25) Smith, S. R.; Neyhart, G. A.; Kalsbeck, W. A.; Thorp, H. H. *New J. Chem.* **1994**, *18*, 397-406.